Nanoscale Advances

Accepted Manuscript

This article can be cited before page numbers have been issued, to do this please use: G. Darabdhara, M. J. Baruah, E. Saikia, S. B. Gohain, R. Bayan, R. Kemprai, D. Gogoi, Y. Park, B. Das and M. Sharma, *Nanoscale Adv.*, 2026, DOI: 10.1039/D5NA01116G.

ROYAL SOCIETY OF CHEMISTRY

rsc.li/nanoscale-advances

View Article Online
DOI: 10.1039/D5NA01116G

Nanoporous $Ni(OH)_2$ Interlinked Co_3O_4 Heterojunction: A Novel Approach to Chromium (VI) Detection

Gitashree Darabdhara,[a] Manash J. Baruah,[b] Eramoni Saikia,[c] Shivanee Borpatra Gohain,[d] Rajarshi Bayan,[e] Rahul Kemprai,[f] Dipankoj Gogoi,[g] Young-Bin Park,[h] Biraj Das,[b,*] Mukesh Sharma[e,*]

[a]*Department of Chemistry, Jagannath Barooah University, Jorhat, Assam, India 785001*
[b]*Department of Chemistry, D. C. B. Girls College, Jorhat, Assam, India, 785001*
[c]*Department of Chemistry, D. D. R. College, Chabua, Dibrugarh, Assam, India, 786184*
[d]*Department of Chemistry, Dimoria College (Autonomous), Khetri, Kamrup(M), Guwahati, Assam, India, 782403*
[e]*Department of Chemistry, Arya Vidyapeeth College (Autonomous), Guwahati, Assam, India, 781016*
[f]*Department of Chemistry, Suren Das College (Autonomous), Hajo, Kamrup, Assam, India, 781102*
[g]*Department of Chemistry, D. H. S. K. College (Autonomous), Dibrugarh, Assam, India, 786001*
[h]*Department of Mechanical Engineering, Ulsan National Institute of Science and Technology, UNIST-gil 50, Ulju-gun, Ulsan 44919, Republic of Korea*

Abstract

The present study broadly explores the synthesis, structural characteristics, and electrochemical performance of nanoporous $Ni(OH)_2/Co_3O_4$ heterojunction engineered for efficient enzymatic sensing of hexavalent chromium Cr(VI). The synthesized heterostructure consists of a porous $Ni(OH)_2/Co_3O_4$ matrix (nanopores, with dimensions approximately ranging from 6 to 10 nm) intimately coupled with evenly dispersed Co_3O_4 nanocrystals, forming a well-integrated interface that enables strong synergistic redox coupling and rapid electron transport across the junction. The nanoporous framework significantly increases the electrochemically active surface area offering abundant catalytic active sites, and facilitates improved transport of electrolytes. Simultaneously, the heterojunction ensures continuous conductive pathways, thereby minimizing charge-transfer resistance and enhancing overall electron mobility. The combined structural and electronic advantages translate into markedly improved sensitivity, catalytic activity, and operational stability for enzymatic Cr(VI) detection with a limit of detection (LOD) of 39 nm. Overall, the results underscore the

View Article Online
DOI: 10.1039/D5NA01116G

significant role of heterojunction engineering in enhancing the performance of metal hydroxide-oxide materials for advanced environmental sensing applications.

Keywords: Nanoporous, $Ni(OH)_2/Co_3O_4$, Cr(VI) detection, TMB oxidation

1. Introduction

Hexavalent chromium (Cr(VI)) is a highly toxic and carcinogenic pollutant prevalent in industrial effluents, posing significant environmental and health risks. Its reduction to the less toxic trivalent chromium (Cr(III)) and accurate sensing are crucial for environmental remediation and monitoring. The reduction of Cr(VI) to the less harmful Cr(III) is a critical process in detoxifying contaminated water. Chronic exposure to Cr(VI) causes bronchitis, liver, kidney, and nerve tissue damage, and it has been shown to have carcinogenic, mutagenic, and genotoxic effects.[1,2] While the U.S. Environmental Protection Agency (EPA) says that 0.1 mg L^{-1} is the permissible quantity, the World Health Organization (WHO) recommends a tolerable value of 0.050 mg L^{-1} for Cr in drinking water.[3-5] Thus, rapid and effective Cr(VI) detection technology is essential to drinking water sources and food safety. When it comes to sensing, common detection techniques include X-ray fluorescence, voltammetry, spectrofluorometry, spectrophotometry (colorimetric), inductively coupled plasma atomic emission spectrometry or mass spectroscopy, and graphite furnace atomic absorption spectrometry.[6] Despite their extremely high sensitivity, optical atomic spectrometry and mass spectroscopy are incompatible with on-site detection and necessitate highly skilled individuals and expensive, complicated equipment to perform. Analyte detection via colorimetric techniques is one of the most popular approaches due to its ease of use, particularly when it involves a color shift that is visible to the unaided eye. Nanozymes are a class of nanomaterials that, because of their inherent characteristics-such as size, structure, surface charge, etc. can effectively mimic normal enzymes by catalyzing H_2O_2-mediated reactions.[7,8] For instance, Cr(VI) was detected and quantified utilizing gold

View Article Online
DOI: 10.1039/D5NA01116G

amalgam nanocomposites with oxidase capabilities and 3,3′,5,5′ - tetramethylbenzidine (TMB) as a substrate.[5] Using polyethylenimine-stabilized Ag nanoclusters, oxidation of TMB by Cr (VI) was employed in a different investigation to detect the same with a broader linearity range of 0.25-5.2 mg L^{-1} and a LOD and LOQ of 0.0572 and 0.1924 mg L^{-1}, respectively.[9] Similarly, in the presence of TMB and H_2O_2, polyethylene glycol-functionalized poly(Nphenyl glycine) (PNPG-PEG) nanoparticles were employed to improve the signal for the detection of Cr(VI).[10] Good linearity (0.01-0.1 μM) and LOD (0.012 μM) were attained using the approach. Because of its potent anti-interference properties, non-toxicity, and excellent stability, TMB has been used as a chromogenic chemical in a number of other investigations.[11,12]

The detection of Cr(VI) has significantly advanced with the recent developments in nanozyme-based sensing platforms that includes use of defect-engineered single-atom catalysts, MOF-based oxidoreductase mimics, and fluorescent carbon nanodots.[13-16] Despite of their significant sensitivity, many systems suffer from poor structural withstanding capability in acidic environments, high substrate affinity constants, aggregation-induced deactivation, and restricted electron-transfer efficiency.[17] Furthermore, there is still a lack of research on smartly designed engineered nanoporous heterojunctions that optimize accessibility to the catalytic site and interfacial redox coupling. Therefore, by improving charge transfer, enhancing active site density, and boosting catalytic kinetics for effective Cr(VI) detection, the development of a structurally integrated $Ni(OH)_2/Co_3O_4$ nanoporous heterojunction offers a promising strategy to overcome these limitations.

Bimetallic metal oxides play a crucial role in the sensing and reduction of Cr(VI) due to their enhanced catalytic, electrochemical, and adsorption properties.[18] The incorporation of two different metals into the metal oxide framework often results in synergistic effects that

View Article Online
DOI: 10.1039/D5NA01116G

improve performance in environmental applications, particularly in the detection and detoxification of Cr(VI).[19]

The presence of two metals in a metal oxide matrix can create more active sites and enhance electron transfer processes, which are essential for the reduction of Cr(VI).[20] Furthermore, the combination of two metals increases the adsorption capacity for Cr(VI), attributed to the varied oxidation states and coordination environments that bimetallic oxides offer.[21] This enhancement in adsorption is crucial for capturing Cr(VI) ions from contaminated water. Nanoporous heterojunctions based on bimetallic oxides have emerged as promising candidates for Cr(VI) sensing and reduction due to their unique structural and electronic properties.[22] The heterojunction formation facilitates efficient electron transfer, essential for the reduction process. Moreover, the stability and durability of bimetallic oxides in harsh conditions are crucial for practical applications in water treatment and environmental remediation.[22]

In addition to conventional catalytic and nanozyme-based sensing techniques, semiconductor photocatalysis has become a successful method for monitoring pollutants and environment remediation. Cr(VI) can be degraded more easily with the help of photocatalytic materials, which produce reactive oxygen species owing to photoinduced charge separation.[20,22] Recent developments in plasmonic and hot electron photocatalysis have additionally expanded the opportunity of catalytic nanomaterials *via* enabling effective utilization of light energy through localized surface plasmon resonance (SPR) and energetic charge carriers.[23] Hot-electron-mediated processes can greatly improve interfacial redox reactions by enhancing charge injection and suppressing recombination losses.[23,24] These new concepts emphasize the effectiveness of electron-transfer routes and interfacial charge transport in catalytic nanostructures.[25,26]

View Article Online
DOI: 10.1039/D5NA01116G

While our present work is focused on colorimetric sensing using nanozymes rather than photocatalysis, the design of nanoporous $Ni(OH)_2/Co_3O_4$ heterojunctions is fundamentally similar to photocatalytic systems in terms of heterointerface-driven charge separation and improved catalytic activity. By optimizing the interface between $Ni(OH)_2/Co_3O_4$, we enable competent electron transfer pathways that are vital for both nanozymatic oxidation of TMB and the potential photocatalytic detoxification of industrial effluents.

Highlighting the critical role of nanoporous materials, this article explores the synthesis, characterization, and catalytic capabilities of nanoporous $Ni(OH)_2/Co_3O_4$ heterojunction in Cr(VI) sensing. Employing a multidisciplinary approach spanning chemistry, materials science, and environmental engineering, this research aims to advance the development of efficient, sustainable strategies for mitigating hazardous pollutants and safeguarding environmental integrity. The novelty of the present work lies in the rational design of a nanoporous $Ni(OH)_2/Co_3O_4$ heterojunction that integrates interfacial redox coupling with high-surface-area nanoarchitecture to enhance peroxidase-like catalytic performance. In contrast to previously documented mono-metallic or randomly built bimetallic nanozymes, the developed interface enables faster electron passage between Ni^{2+} and Co^{2+}/Co^{3+} centres that contributes towards improving the formation of reactive oxygen species which helped in the detection of Cr(VI). Heterojunction-mediated charge transport in combination with nanoporous morphology offers an exclusive catalytic intensification method for stable and sensitive Cr(VI) colorimetric detection.

2. Materials and Methods

2.1.Materials

Cobalt chloride ($CoCl_2$) and nickel chloride ($NiCl_2.6H_2O$) were purchased from E-Merck, India. Sodium hydroxide (NaOH) was brought from E-Merck. 4-nitrophenol and sodium

View Article Online
DOI: 10.1039/D5NA01116G

borohydride ($NaBH_4$) were received from Sigma-Aldrich, Germany. $K_2Cr_2O_7$ was purchased from E-Merck, India. 3,3',5,5'-tetramethylbenzidine (TMB) was purchased from Sigma Aldrich, USA. All the chemicals were used as received and without any further purification.

2.2.Instrumental Techniques

The Fourier-transform Infrared Spectroscopy spectrum (FT-IR) was recorded in the mid-IR range of 450-4000 cm^{-1} in a Frontier-MIR-FIR from Perkin-Elmer. The FT-IR of solid samples were recorded in DRIFT mode by grinding the samples with KBr. Powder X-ray diffraction (PXRD) measurement was recorded in BRUKER AXS, D8 FOCUS instrument in a low angle measurement from 2θ values of 10–80°. Raman analyses were done on Horiba LabRAM HR spectrophotometer equipped with a He-Ne laser of excitation wavelength of 514.5 nm. The electronic absorption spectrum was recorded using a SHIMADZU UV-2600i spectrophotometer. The XPS analysis was carried out on ESCALAB Xi+ Make: Thermo Fisher Scientific Pvt. Ltd., UK Model: A UV/Visible spectrophotometer (SPECORD-200, Analytikjena, Germany) was used to measure the produced nanocomposite's peroxidase activity toward Cr(VI) detection.

2.3.Synthesis of bimetallic nanocatalyst, $Ni(OH)_2/Co_3O_4$

To synthesize the nanocatalyst, 14.4 mg of nickel chloride ($NiCl_2.2H_2O$) is dissolved in 100 mL of water. A concentrated solution of sodium hydroxide (NaOH) is then added until complete precipitation of nickel hydroxide, $Ni(OH)_2$, occurs. The resulting precipitate is washed several times with hot water and subsequently dried in an oven. Next, the dried $Ni(OH)_2$ precipitate is meticulously mixed with 7.5 mg of cobalt chloride ($CoCl_2$) in a mortar and pestle for 8 h. The resulting mixture is washed repeatedly with hot water to eliminate any impurities present, followed by drying in an oven at 100°C to obtain the final bimetallic $Ni(OH)_2/Co_3O_4$ nanocatalyst, Scheme 1.

View Article Online
DOI: 10.1039/D5NA01116G

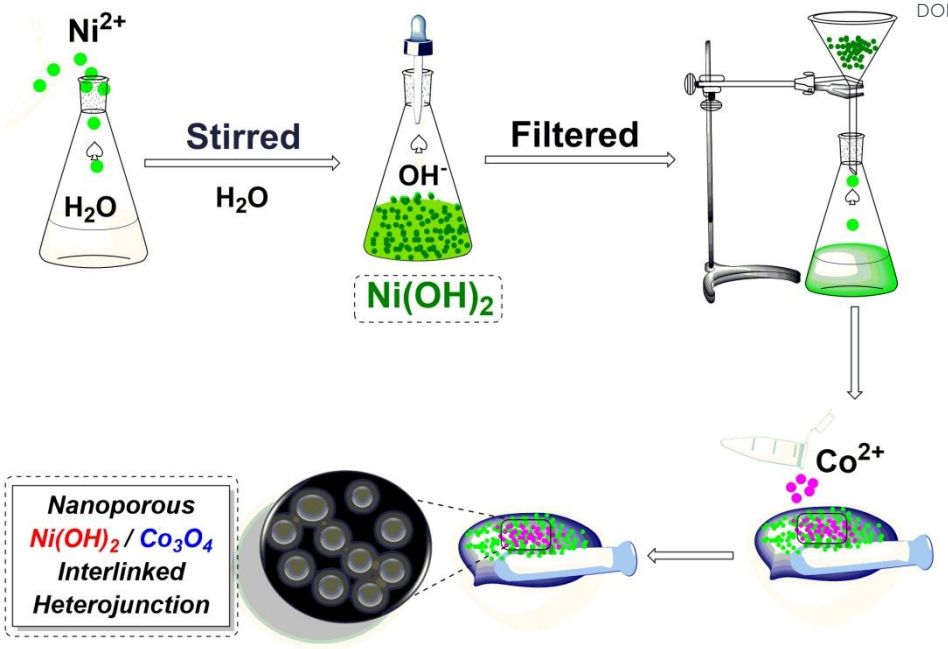

Scheme 1. A schematic illustration for the synthesis of $Ni(OH)_2/Co_3O_4$

2.4.Investigation of $Ni(OH)_2/Co_3O_4$ peroxidase-like properties

Chromogenic TMB molecules are effectively oxidized by the $Ni(OH)_2/Co_3O_4$ to produce oxidized blue-colored TMB product (Ox-TMB). The standard procedure involved adding 100 µL of $Ni(OH)_2/Co_3O_4$ (50 mg/L) to a 0.5 mM TMB solution in an acetate buffer of pH 4. After adjusting the reaction mixture's volume to 3 mL and adding 50 µL of H_2O_2 (30%) solution, the mixture was incubated for 20 min at 25 ^oC in a water bath shaker. The Ox-TMB product was monitored using a UV-visible spectrophotometer at λ_{max} value of 652 nm. Different parameters such as the concentration of $Ni(OH)_2/Co_3O_4$, pH of the reaction and temperature was investigated. Next, the temperature and initial pH of the reaction mixture were changed in order to examine the TMB oxidation processes.

By adjusting TMB and H_2O_2 within a specific concentration range, typical Michaelis-Menten curves for the $Ni(OH)_2/Co_3O_4$ nanocomposite were produced. The Michaelis-Menten

View Article Online
DOI: 10.1039/D5NA01116G

constant (K_m) and the Lineweaver-Burk double reciprocal plot were used to calculate the enzyme's affinity for the substrate. The Lineweaver-Burk plot uses the following equation:

$$\frac{1}{v} = \left(\frac{Km}{Vm}\right)\left(\frac{1}{[S]}\right) + \left(\frac{1}{Vm}\right) \quad \text{(Equation 1)}$$

where v = initial velocity; V_m = maximal reaction velocity and [S] = substrate concentration.

2.5. Colorimetric detection of Cr(VI) in aqueous solution

The detection of Cr(VI) in aqueous media was used to investigate the nanozymatic detection activity of $Ni(OH)_2/Co_3O_4$ nanocomposite. Separate additions of Cr(VI) (50-500 nM concentrations) were made to the reaction mixture which contained 50 µL H_2O_2 (30%) in a buffer solution of pH 3, 0.5 mM TMB, and 100 µL $Ni(OH)_2/Co_3O_4$ nanocomposite. Following this, the analysis of the Cr(VI) detection was done using changes in UV-vis absorbance intensities at 652 nM for the Ox-TMB product. In order to investigate the selectivity of $Ni(OH)_2/Co_3O_4$ nanocomposite, 200 nM of various interfering ions, namely Pb(II), Na(I), Cu(II), Hg(II), As(III), K(I), Cd(II), and Co(II), were added to the reaction mixture in a manner as described above.

3. Results and Discussion

3.1. Characterization of $Ni(OH)_2/Co_3O_4$ heterojunction

Transmission electron microscopy (TEM) was employed to assess the crystallinity and confirm the morphology of the synthesized $Ni(OH)_2/Co_3O_4$ heterojunctions. The TEM images presented in Fig. 1 illustrates the nanoporous morphology of the $Ni(OH)_2/Co_3O_4$ nanocomposite, with $Ni(OH)_2$ interlinked with Co_3O_4 nanocrystals. Fig. 1a-c demonstrate a homogenous formation of nanopores, with dimensions approximately ranging from 6 to 10 nm, clearly showcasing the heterojunction structures. High-resolution TEM (HRTEM) analysis (Fig.1d) reveals an interplanar spacing of about 0.24 nm, which corresponds to the spacing between the (311) crystal planes of the $Ni(OH)_2/Co_3O_4$ nanocomposite.[27] This

View Article Online
DOI: 10.1039/D5NA01116G

interplanar spacing is indicative of the crystalline nature and confirms the successful synthesis of the heterojunction material, which is also supported by the SAED pattern of the synthesised material (inset of Fig. 1d). We have calculated the average crystallite size of the nanoporous $Ni(OH)_2$ interlinked Co_3O_4 heterojunction using the Scherrer equation based on the XRD data provided.[28,29]

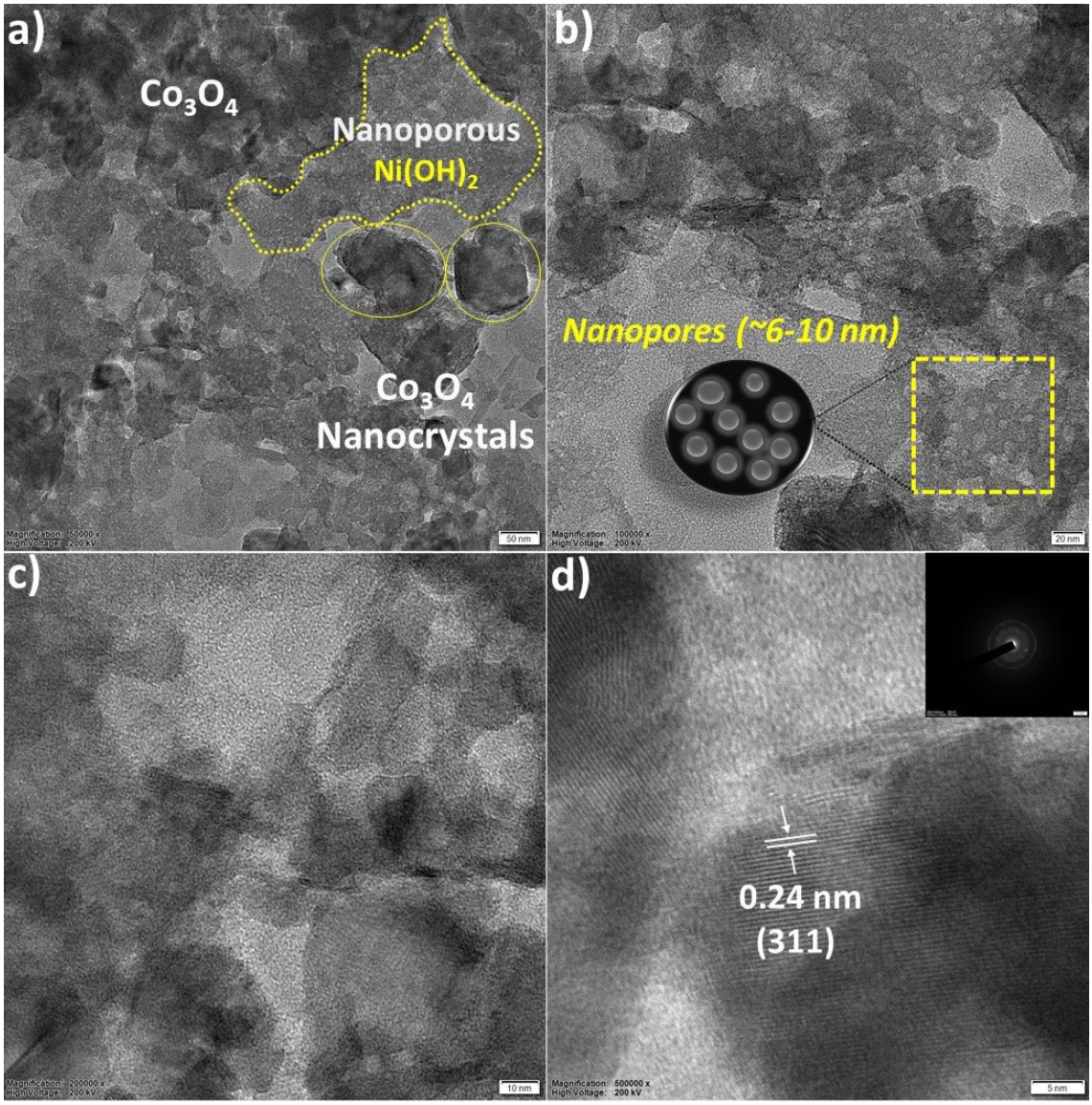

Fig. 1 TEM images of the synthesized $Ni(OH)_2/Co_3O_4$ heterojunctions. (a-c) formation of nanopores in the dimension range of ~6-10 nm, illustrating the interconnected structure. (d) HRTEM image showing an interplanar spacing of about 0.24 nm (inset of (d) shows the selected area electron diffraction, SAED pattern).

View Article Online
DOI: 10.1039/D5NA01116G

This calculated value is in exact agreement with the TEM analysis, which shows a homogenous formation of nanocrystals and nanopores with dimensions ranging from 6 to 10 nm. The calculated size supports the HRTEM observation of an interplanar spacing of 0.24 nm for the (311) crystal planes, confirming high crystallinity within these small domains.

These findings are significant as they underscore the nanoporous architecture of the synthesized material, which is crucial for enhancing the catalytic activities.

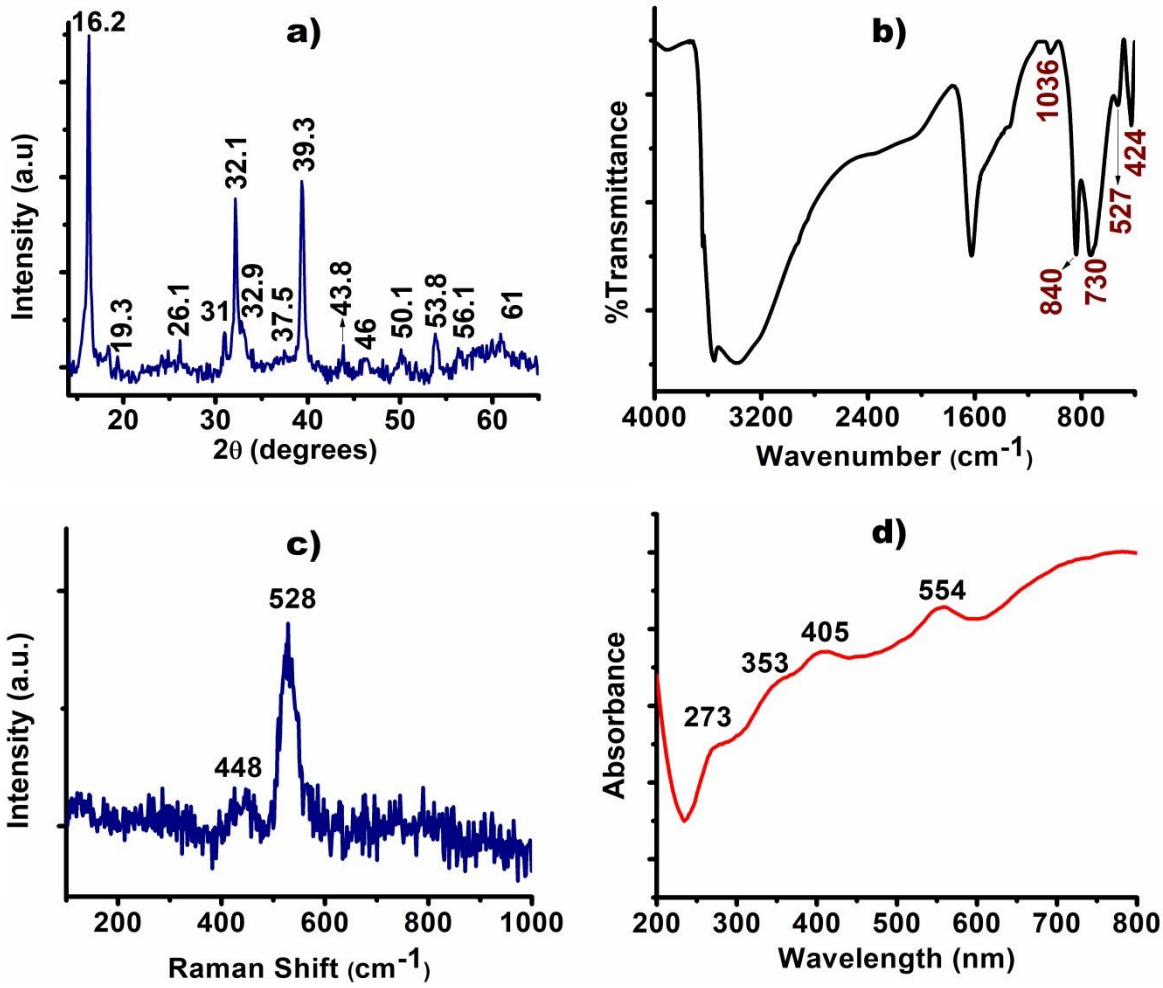

Fig. 2. a) XRD, b) FT-IR, c) Raman and d) UV-DRS analysis of $Ni(OH)_2/Co_3O_4$ nanocomposite

View Article Online
DOI: 10.1039/D5NA01116G

In the XRD spectra, the peaks were observed at 31, 39.3, 43.8 and 56.1 corresponding to Co_3O_4 and peaks for $Ni(OH)_2$ were observed at 2θ values of 37.5, 46, and 61 as shown in Fig. 2a.[27,30] In the FT-IR spectra, the peaks appeared at 418 cm^{-1} for the Ni-O stretching band of $Ni(OH)_2$. Besides this, vibrational bands found at 530 cm^{-1} for Co^{2+}-O and 730 cm^{-1} for Co^{3+}-O of the Co_3O_4 unit of the material for the octahedral and tetrahedral sites of the Co_3O_4 unit in spinel structure, Fig. 2b.[27,31] The Raman spectra of the synthesized $Ni(OH)_2/Co_3O_4$ clearly displays peaks at 448 and 528 cm^{-1}, which evidently demonstrate the presence of both Ni-O and Co_3O_4 unit in the $Ni(OH)_2/Co_3O_4$ composite, Fig. 2c.[27] From the UV-DRS spectra, the absorption peaks appeared at 273 nm corresponds to $O^{2-} \rightarrow Co^{2+}$ and that at 554 nm for the $O^{2-} \rightarrow Co^{3+}$ charge transfer transition of the Co_3O_4 unit.[32,33] Peaks observed at 353 and 405 nm could be attributed for Ni-O transition in $Ni(OH)_2$ NPs, Fig. 2d.[34]

The crystalline nature and phase purity of the nanoporous $Ni(OH)_2/Co_3O_4$ heterojunction were evaluated using PXRD and TEM-SAED analysis. The average crystallite size was calculated to be approximately ~9.5 nm using the Scherrer equation and the detailed calculation is provided in the ESI.[35] This is in excellent agreement with the TEM observations, which reveal interlinked nanocrystals and nanopores within the 6-10 nm range. The calculated size supports the HRTEM observation of an interplanar spacing of 0.24 nm for the (311) crystal planes, confirming high crystallinity within these small domains.[36,37]

Based on X-ray Photoelectron Spectroscopy (XPS) spectra, the presence of Co and Ni was confirmed based on distinctive peaks and binding energies. Binding energies values found at 856.3 eV for $2p_{3/2}$ and 873.9 eV for $2p_{1/2}$, corresponding to Ni^{2+} in $Ni(OH)_2$.[38] The satellite peaks were appearance at 862.1 eV and 880.6 eV further supports the presence of NiO, Fig. 3a.[39] Binding energies values observed at 781.6 eV and 798.1 eV for $2p_{3/2}$ and $2p_{1/2}$, respectively, indicating the presence of Co^{2+} and after deconvolution peak at 796.5 eV for the

View Article Online
DOI: 10.1039/D5NA01116G

presence of Co^{3+} in the synthesized material.[40] The satellite peaks were observed at 786.1 eV and 803.2 eV were characteristic for the spinal structure of the synthesized material which also confirmed form FTIR analysis, Fig. 3b.[40] These findings confirm the formation of Co_3O_4 and $Ni(OH)_2$ in the analysed sample, providing valuable insight into its chemical composition and structure. Zhao *et al*. also observed similar binding energy values in the spinal structure of the synthesized Co_3O_4 nanostructures.[41] In the oxygen (O) spectra of the synthesized material, two peaks appeared after deconvolution at 530.7 eV and 531.5 eV, indicative of different O binding sites, Fig. 3c.[42] The peak found at 530.7 eV for the presence of metal oxide formation and binding energy values at 531.5 eV for oxygen vacancies.[42] Carbon (C) spectra of the material revealed two peaks at binding energy values of 284.7 eV for C-C bonds and 286.0 eV for the presence of O-C=O groups, respectively, Fig. 3d.[40]

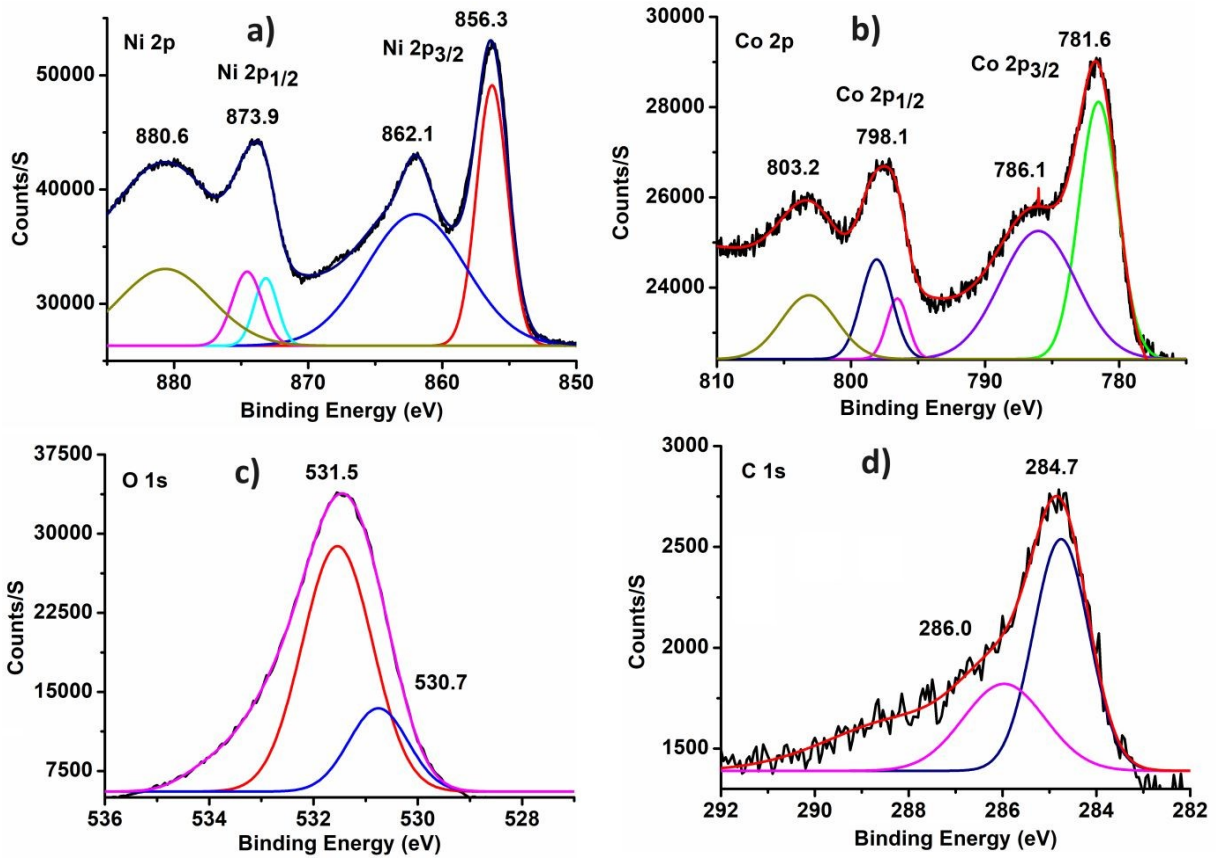

Fig. 3. XPS spectra of (a) Ni 2p, (b) Co 2p, (c) O 1s, and (d) C 1s of the synthesized $Ni(OH)_2/Co_3O_4$ nanocomposite

View Article Online
DOI: 10.1039/D5NA01116G

3.2.$Ni(OH)_2/Co_3O_4$ nanocomposite's intrinsic peroxidase-like activity and reaction condition optimization

The oxidation reaction of TMB in the presence of H_2O_2 was used to investigate the peroxidase-like activity of the $Ni(OH)_2/Co_3O_4$ nanocomposite. The resulting blue colored oxidized product of TMB showed absorbance maxima at 652 nm due to the formation of 3,3′,5,5′-tetramethylbenzidine diimine (TMBDI).[43]

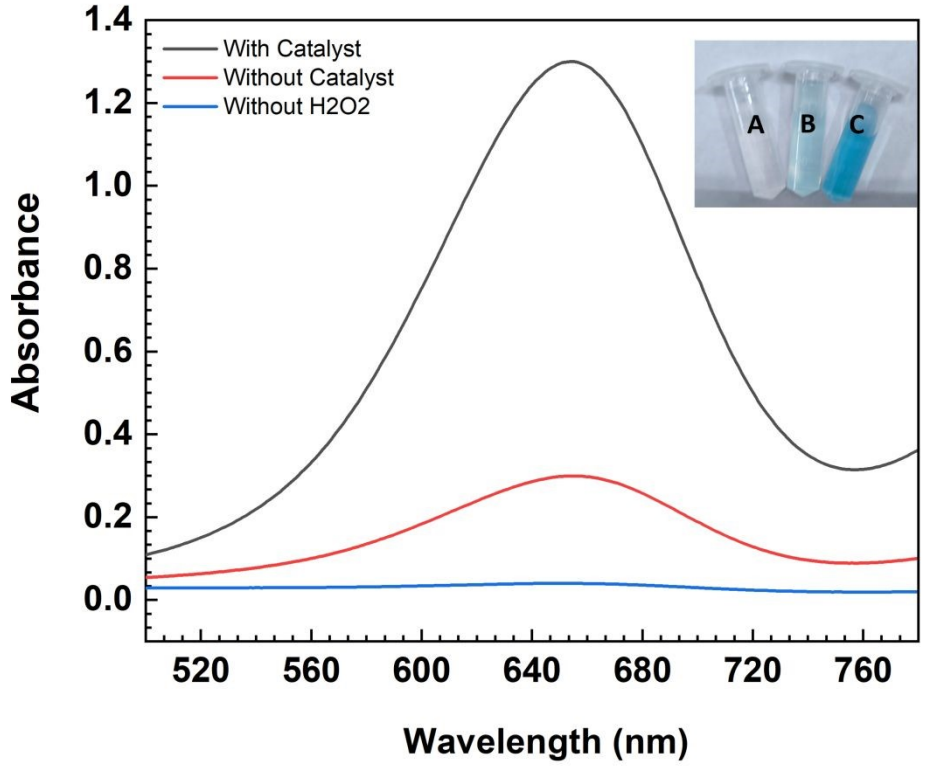

Fig. 4. UV-visible spectrum of 0.5 mM TMB without H_2O_2, without $Ni(OH)_2/Co_3O_4$ nanocomposite and in presence of both H_2O_2 and $Ni(OH)_2/Co_3O_4$ nanocomposite. The inset shows the corresponding photographs (A=without H_2O_2; B=without $Ni(OH)_2/Co_3O_4$ nanocomposite but in presence of H_2O_2; C=presence of both $Ni(OH)_2/Co_3O_4$ nanocomposite and H_2O_2)

To illustrate the $Ni(OH)_2/Co_3O_4$ nanocomposite's peroxidase-like catalytic activity, the oxidation of TMB was investigated under various conditions. $Ni(OH)_2/Co_3O_4$ nanocomposite-catalyzed TMB oxidation was carried out as a control without H_2O_2. Since

View Article Online
DOI: 10.1039/D5NA01116G

there was no color change, it can be concluded that TMB oxidation requires both H_2O_2 and the $Ni(OH)_2/Co_3O_4$ nanocomposite. The peroxidase like catalytic activity towards TMB oxidation was found to be significantly higher when the reaction was conducted in presence of the catalyst as well as H_2O_2. The changes observed due to the oxidation of TMB is depicted in Fig. 4 below.

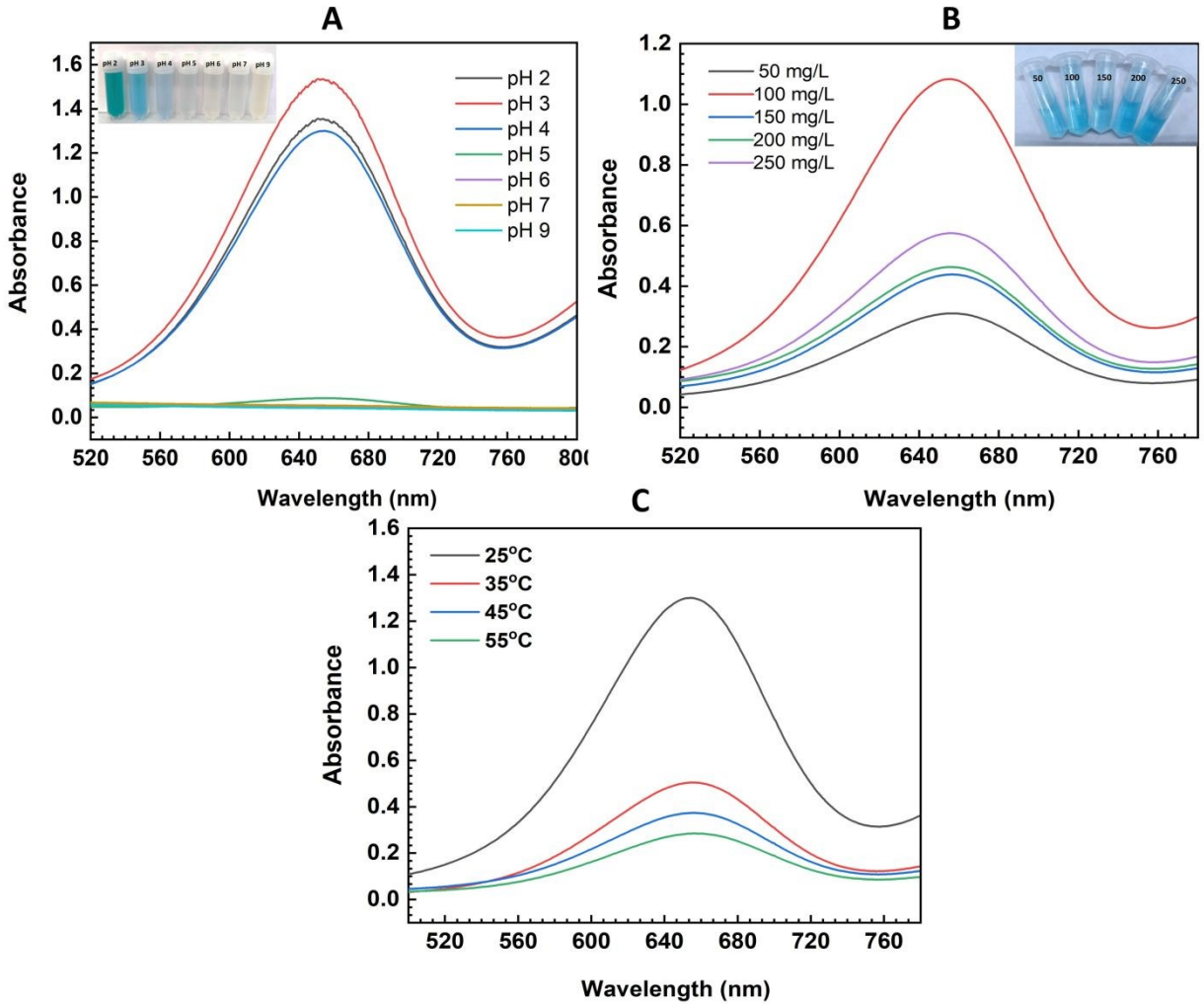

Fig. 5. UV-visible absorption spectra for oxidation of TMB using $Ni(OH)_2/Co_3O_4$ nanocomposite with varying (A) pH, (B) catalyst concentration and (C) temperature.

It was possible to choose the ideal analytical conditions by examining how the pH, temperature, and catalyst quantity affected the peroxidase-like activity of the $Ni(OH)_2/Co_3O_4$ catalyst. Fig. 5A shows how pH affects the activity of the $Ni(OH)_2/Co_3O_4$ catalyst. The

View Article Online
DOI: 10.1039/D5NA01116G

catalytic activity of $Ni(OH)_2/Co_3O_4$ quickly declines beyond pH 3, which is also the pH at which maximum absorbance is seen. At a concentration of 100 mg L^{-1} of $Ni(OH)_2/Co_3O_4$ nanocomposite, the maximum catalytic activity was observed at 25 °C (Fig. 5B, 5C). Thus, the following circumstances result in the highest catalytic activity: 100 mgL^{-1} of $Ni(OH)_2/Co_3O_4$ nanocomposite at pH 3 and 25 °C.

3.3.Kinetic evaluation of $Ni(OH)_2/Co_3O_4$ nanocomposite as peroxidase mimic and determination of Michaelis constant

Utilizing steady state kinetics and the initial rate approach, the intrinsic peroxidase-like catalytic activity of the $Ni(OH)_2/Co_3O_4$ nanocomposite was examined utilizing TMB and H_2O_2 as substrates. While maintaining a constant concentration of the other reagents, kinetic analysis was carried out by varying the concentration of the substrates (TMB and H_2O_2). Beer Lambert's law was used to convert the absorbance readings to their respective concentrations:

$A = \varepsilon_{TMBDI} \times c \times L$……(**Equation 2**)

where ε_{TMBDI} = 39000 $M^{-1}cm^{-1}$ at 652 nm for TMBDI, c=concentration of the sample and L refers to the path length.[44]

Typical Michaelis Menten curves for TMB and H_2O_2 (shown in Fig. 6A and 6B, respectively), as substrates in a certain concentration range, were produced by converting the appropriate concentration terms to velocity terms. Lineweaver Burk double reciprocal plots were then used to determine the catalytic parameters K_m (Michaelis constant) and V_m (maximal velocity) of the enzyme mimics $Ni(OH)_2/Co_3O_4$. The slope of the Lineweaver Burk double reciprocal plots' (as shown in the insets of Fig. 6A and 6B) yields the value of K_m, while their intercept yields the value of V_m. The K_m value of $Ni(OH)_2/Co_3O_4$ for TMB as substrate was found to be 0.53 mM whereas that for H_2O_2 was found to be 2.42 mM. The corresponding V_m values for TMB and H_2O_2 as substrates was found to be 4.77×10^{-8} Ms^{-1} and 2.80×10^{-8} Ms^{-1}, respectively.

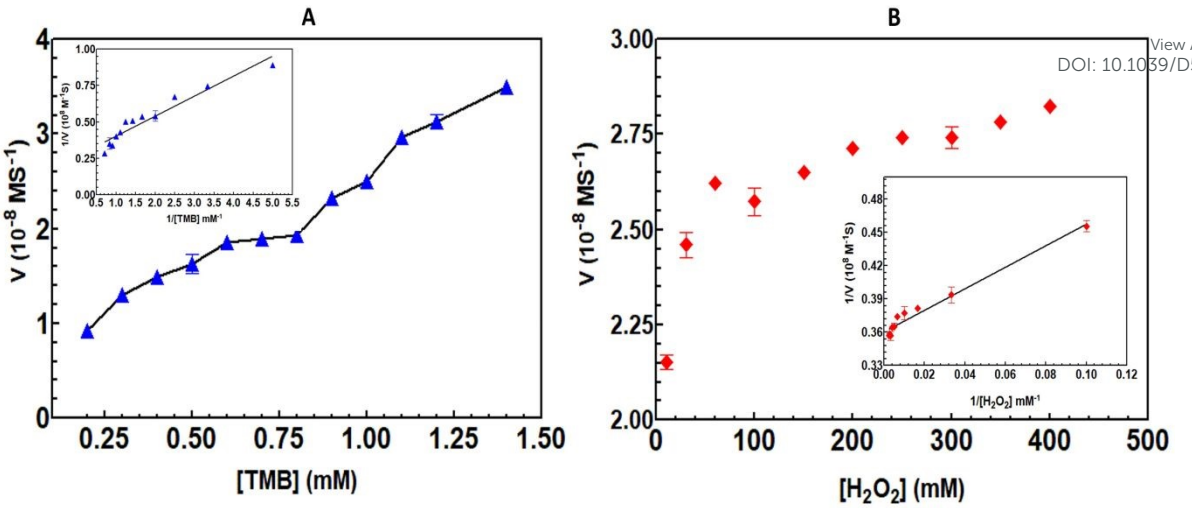

Fig. 6. $Ni(OH)_2/Co_3O_4$ nanocomposites' catalytic mechanism and steady-state kinetic assay. (A) TMB concentration variation at a fixed H_2O_2 concentration (50 mM). (B) H_2O_2 concentration variation at a fixed TMB concentration (0.5 mM). The inset displays the matching Lineweaver–Burk plots of the double reciprocal of the Michaelis Menten equation.

The low K_m value (0.53 mM for TMB) for $Ni(OH)_2/Co_3O_4$ suggests that it has a higher substrate affinity for TMB. Additionally, compared to many other enzyme mimics as shown in Table S1, the K_m value reported for $Ni(OH)_2/Co_3O_4$ with H_2O_2 is significantly lower, indicating that a lower H_2O_2 concentration is needed for TMB oxidation.

3.4.Plausible mechanism of the peroxidase like activity

The pertinent reactive species in the catalytic system were observed in order to examine the catalytic mechanism of the peroxidase-like activity of the $Ni(OH)_2/Co_3O_4$ nanocomposites. The peroxidase-like activities of nanozymes catalyse the generation of hydroxyl radicals (•OH) from hydrogen peroxide (H_2O_2), which in turn oxidize the chromogenic substrate to produce the blue colour. $Ni(OH)_2/Co_3O_4$ nanocomposites exhibit strong peroxidase-mimicking activity as a result of their Fenton-like behavior in the presence of H_2O_2. TMB molecules are adsorbed onto the surface of the $Ni(OH)_2/Co_3O_4$ nanocomposites. The adsorption of TMB molecules onto the surface of the $Ni(OH)_2/Co_3O_4$ nanocomposites surface

View Article Online
DOI: 10.1039/D5NA01116G

occurs through π–π interactions between their functional groups. $Ni(OH)_2/Co_3O_4$ facilitates Fenton reactions that generate •OH radicals from H_2O_2. The reactions involved in the Fenton process is shown in the equations below (Equation 3 to 5).[45,46]

Co_3O_4 has mixed valence states (Co^{2+} and Co^{3+}) that accelerate Fenton-like reactions to break down H_2O_2.

$Co^{2+} + H_2O_2 \longrightarrow Co^{3+} + OH^- + {}^{\cdot}OH$……(**Equation 3**)

$Co^{3+} + H_2O_2 \longrightarrow Co^{2+} + H_2O + HOO^{\cdot}$……(**Equation 4**)

The ·OH radical, being a powerful oxidizing species, converts TMB into blue-colored Ox-TMB, which exists in equilibrium with the cation free radical TMB^{+}•.

TMB + ·OH ⟶ ox-TMB (blue colour)....…….(**Equation 5**)

Although we could not quantify the decomposition of H_2O_2 (as it was used in a significantly lesser amount, 50 µL), but its role in generation of •OH can be evaluated using a fluorescent method using terephthalic acid (TA) as a probe molecule. TA reacts selectively with •OH to form 2-hydroxyterephthalic acid (TAOH) that shows a characteristic fluorescence emission at 410 nm. The excitation and emission wavelengths are at 315 nm and 410 nm, respectively. The fluorescence signal of TAOH confirms the formation of •OH in the reaction system. In a typical experiment, optimized amount of the catalysts (100 mgL^{-1}) was dispersed in an aqueous TA/NaOH solution (1:2 molar ratio) containing 50 µL H_2O_2. The fluorescence spectra were recorded at 5 min and 20 min (as shown in Fig. S1, in SI). The enhanced PL intensity at 20 min indicates a more efficient generation of •OH compared to that at 5 min. Since fluorescence intensity at 410 nm is directly proportional to •OH production, the stronger emission confirms higher •OH generation, leading to faster and more efficient TMB oxidation.

3.5.Detection of Cr(VI) using $Ni(OH)_2/Co_3O_4$ nanocomposites and Selectivity study

View Article Online
DOI: 10.1039/D5NA01116G

The nanozymatic detection technique has garnered significant attention in the last years because of its simplicity, convenience of use without a sophisticated instrument, and visibility to the unaided eye.[47] Accordingly, $Ni(OH)_2/Co_3O_4$ nanocomposites was also effectively used for the colorimetric detection of Cr(VI) due to its superior peroxidase-like activity, as was previously mentioned.

Typically, in acetate buffer of pH 3, $Ni(OH)_2/Co_3O_4$ nanocomposites, H_2O_2 (30%) and TMB in their optimum conditions, were allowed to mix with varying quantities of freshly prepared Cr(VI) solutions (1-300 nM) and allowed to react with the reaction mixture at 25 °C. At a wavelength of 652 nm, the Ox-TMB product's UV-Vis absorbance variations were observed for these various Cr(VI) concentrations. As the concentration of Cr(VI) rose, the absorbance intensity for the OxTMB product increased progressively. In an acidic media, Cr(VI) can break down H_2O_2 into O_2 and H_2O. Fenton reactions allow both O_2 and H_2O to combine with electrons on the surface of $Ni(OH)_2/Co_3O_4$ to form •OH. As a result, when Cr(VI) is present in the reaction mixture, TMB oxidation rises.[48] The absorbance at 652 nm vs. concentration of Cr(VI) was plotted to create a calibration curve based on the variations in absorbance intensity as shown in Fig. 7A. In the linear range of 10-300 nM, the LOD for Cr(VI) detection was found to be 39 nM. Comparing $Ni(OH)_2/Co_3O_4$ activity to the majority of other previously published nanomaterials (Table 1) for colorimetric detection of Cr(VI), the LOD is noticeably lower.

In the presence of 200 nM of various interfering ions, including Hg(II), Pb(II), Cd(II), Cu(II), Co(II), K(I), Na(I), the selectivity of $Ni(OH)_2/Co_3O_4$ was also examined in the colorimetric detection of Cr(VI) as shown in Fig. 7B. The presence of Cr(VI) significantly boosts the TMB oxidation efficiency, most likely as a result of the ions' strong catalytic sites and adsorption at the $Ni(OH)_2/Co_3O_4$ surface. Although not as strongly as with Cr(VI), other

View Article Online
DOI: 10.1039/D5NA01116G

metal ions also interact with the surface of $Ni(OH)_2/Co_3O_4$.[49] When Cr(VI) was present, there was a noticeable rise in the Ox-TMB absorption intensity.

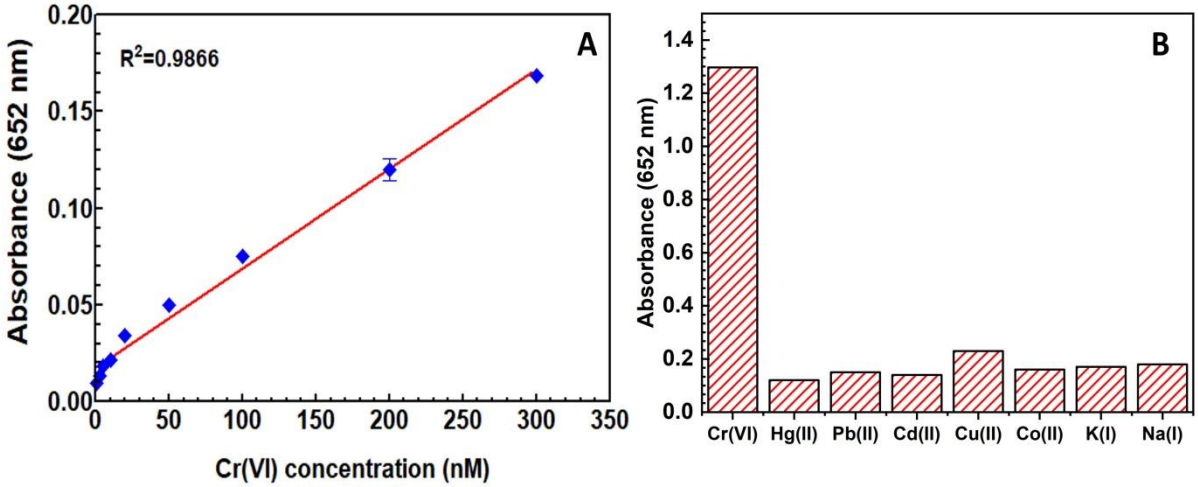

Fig. 7. (A) Standard Cr(VI) concentration response curve under optimum conditions using $Ni(OH)_2/Co_3O_4$ nanocomposite and (B) Selectivity study of Ox-TMB absorbance following the sensing process in the presence of various inorganic ions

Table 1. Evaluation of the activity of $Ni(OH)_2/Co_3O_4$ towards colorimetric Cr(VI) detection activity in comparison to previously published materials

Sl. No.	**Material**	**Linear Range**	**Limit of detection**	**Reference**
1.	N-and S-doped Carbon dots	1-40 µM	0.52 µM	50
2.	Ag-Ag Nanocluster	0.6-10 µM	0.3 µM	51
3.	Graphene QDs	1-500 µM	190 nM	52
4.	CuS/Fe_3O_4	0-1500 µM	60 nM	53
5.	Fe_3O_4@MQDs	0-60 µM	0.26 nM	54
6.	Cu-PyC MOF	0.5-50 µM	0.051 µM	55
7.	PNPG-PEG	0.05-12.5 µM	520 nM	10
8.	$CoFe_2O_4/H_2PPOP$	0.6-100 µM	0.026 µM	56
8.	*$Ni(OH)_2/Co_3O_4$*	10-300 nM	39 nM	*This work*

View Article Online
DOI: 10.1039/D5NA01116G

3.6.Detection of Cr(VI) ion in environmental samples

The synthesized materials' practical sensor application for the detection of the Cr(VI) ion in various environmental samples was examined. Table 2 shows the relative standard deviation and recovery % for the various environmental samples. In several environmental samples, the suggested approach demonstrated a good recovery % for Cr(VI). The findings imply that the suggested sensor can be utilized to detect Cr(VI) in actual samples with good recovery values.

Table 2. Measurement of Cr(VI) in real-world samples

Sample	**Cr(VI) added (nM)**	**Cr(VI) detected (nM)**	**Recovery (%)**
Tap Water	10	9.94	99.40
	50	49.72	99.44
	100	99.50	99.50
Pond Water	10	10.1	101.00
	50	49.20	98.40
	100	98.47	98.47
Well Water	10	9.61	96.10
	50	48.80	97.60
	100	97.52	97.52

3.7.Reusability study of $Ni(OH)_2/Co_3O_4$ nanocomposite

By performing the reaction six times, the reusability of $Ni(OH)_2/Co_3O_4$ nanocomposite as an enzyme-mimic for TMB oxidation was examined. After six catalytic cycles, the relative activity was 84.32% of the initial activity, as illustrated in Fig. 8. According to the results, the $Ni(OH)_2/Co_3O_4$ nanocomposite is a nano-enzyme with superior stability and catalytic activity.

View Article Online
DOI: 10.1039/D5NA01116G

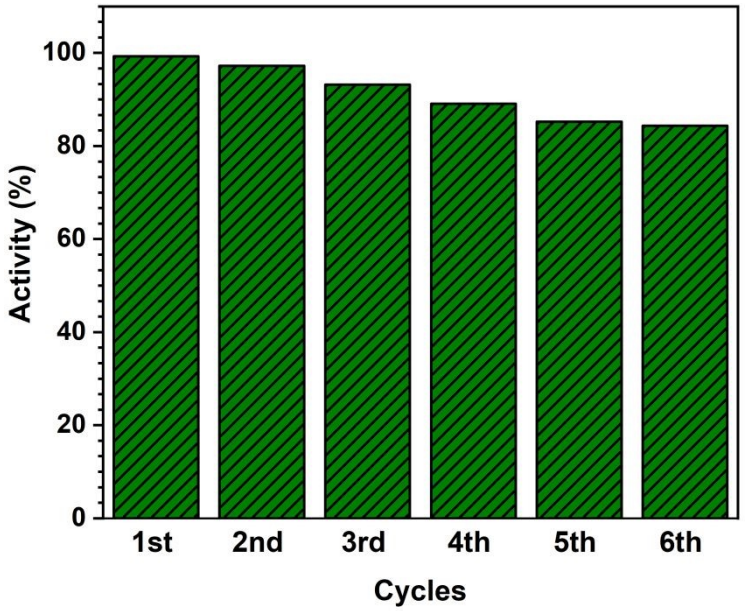

Fig. 8. Reusability study of $Ni(OH)_2/Co_3O_4$ nanocomposite towards TMB oxidation reaction

We have performed a PXRD analysis on the catalyst recovered after five consecutive cycles. The post-catalysis PXRD pattern (now included as Fig. S2 in ESI) shows no significant shift in peak positions or emergence of new phases. This indicates that the heterojunction maintains its structural integrity and phase stability during the sensing of chromium (VI), justifying its excellent reusability. Sensors often face surface poisoning or phase transformation. By showing that the Co_3O_4 and $Ni(OH)_2$ peaks remain unchanged after use, we demonstrate that the detection mechanism is likely surface-redox driven rather than a destructive chemical reaction, confirming the robustness of the material as claimed in the Abstract.

4. Conclusion

In conclusion, we have successfully designed and synthesized a nanoporous $Ni(OH)_2/Co_3O_4$ heterojunction and demonstrated its enhanced peroxidase-like activity for sensitive colorimetric detection of Cr(VI). Integrating engineered heterointerfaces into nanoporous structures has effectively enhanced both catalytic and sensing efficiency. The development of

View Article Online
DOI: 10.1039/D5NA01116G

a distinct heterojunction was confirmed by structural analysis whereas kinetic studies established improved substrate affinity and effective H_2O_2 activation due to synergistic Ni^{2+}-Co^{2+}/Co^{3+} redox coupling. The developed heterojunction delivered a limit of detection of 39 nM, a 10-300 nM linear range and high selectivity for Cr(VI) together with satisfactory stability and reliability in real-sample detection.

This study validates that rational design of heterointerface is crucial in advancing metal hydroxide-oxide catalysts. Connecting the gap between material science and device engineering will be essential for developing the next generation of portable environmental diagnostic tools.

Associated Content

Supporting Information

The supporting information consists of physical measurements of the physicochemical and spectrochemical tools, DRS Spectrum of the FeNi CNPs and catalyst optimization and recyclability graphs.

Author Information

Corresponding Authors:

Dr. Biraj Das- Department of Chemistry, D. D. R. College, Chabua, Dibrugarh, Assam, India, 786184, ORCID: orcid.org/0000-0003-2751-0951, Email: birajdaschm@gmail.com

Dr. Mukesh Sharma- Department of Chemistry, Suren Das College (Autonomous), Hajo, Kamrup, Assam, India, 781102, ORCID: orcid.org/0000-0002-6873-7426, Email: mcotton233@gmail.com.

Authors:

Dr. Gitashree Darabdhara- *Department of Chemistry, Jagannath Barooah University, Jorhat, Assam, India 785001,* Email: gitashree.darabdhara@gmail.com

View Article Online
DOI: 10.1039/D5NA01116G

Dr. Manash J. Baruah- Department of Chemistry, D. C. B. Girls College, Jorhat, Assam, India, 785001, ORCID: orcid.org/0000-0001-8847-4363, Email: manashjbom@gmail.com

Dr. Eramoni Saikia- Department of Chemistry, D. D. R. College, Chabua, Dibrugarh, Assam, India, 786184, Email: eramonisaikia@gmail.com.

Dr. Shivanee Borpatra Gohain- Department of Chemistry, Dimoria College *(Autonomous)*, Khetri, Kamrup(M), Guwahati, Assam, India, 782403, Email: shivaneebgohain@gmail.com

Dr. Rajarshi Bayan- Department of Chemistry, Arya Vidyapeeth College *(Autonomous)*, Guwahati, Assam, India, 781016, Email: rajarshibayan@gmail.com

Rahul Kemprai- Department of Chemistry, Suren Das College *(Autonomous)*, Hajo, Kamrup, Assam, India, 781102

Email: rahulkemprai827@gmail.com

Dipankoj Gogoi- *Department of Chemistry, D. H. S. K. College (Autonomous), Dibrugarh, Assam, India, 786001*
Email: dipankoj2010@rediffmail.com

Professor Young-Bin Park- Department of Mechanical Engineering, Ulsan National Institute of Science and Technology, UNIST-gil 50, Ulju-gun, Ulsan 44919, Republic of Korea, Email: ypark@unist.ac.kr

Conflicts of Interest

There are no conflicts to declare.

Acknowledgments

BD, MS, and MJB sincerely acknowledge DDR College, Dibrugarh, Suren Das College (Autonomous), Kamrup, and DCB Girls College, Jorhat, Assam, India for the analytical facilities provided to perform the experimental works. The authors also thank SAIC-Tezpur University for the instrumentation facilities. GD acknowledges the laboratory facilities of CSIR-NEIST, Jorhat.

View Article Online
DOI: 10.1039/D5NA01116G

View Article Online
DOI: 10.1039/D5NA01116G

References

1 W. Jin and K. Yan, *RSC Adv.,* **2015**, 5(47), 37440–37450. doi:10.1039/c5ra03480a.

2 M. Li and S. Zhou, *Chem. Eng. J.,* **2018**, 339, 539–546. doi:10.1016/j.cej.2018.02.002.

3 M. Loock, J. Beukes and P. Van Zyl, *Water SA,* **2014**, 40(4), 709. doi:10.4314/wsa.v40i4.16.

4 A. Sheikhmohammadi, S. M. Mohseni, R. Khodadadi, M. Sardar, M. Abtahi and S. Mahdavi, *J. Mol. Liq.,* **2017**, 233, 75–88. doi:10.1016/j.molliq.2017.02.101.

5 X. Zhang, W. Liu, X. Li, Z. Zhang and D. Shan, H. *Anal. Chem*., **2018**, 90(24), 14309–14315. doi:10.1021/acs.analchem.8b03597.

6 P. K. Boruah, G. Darabdhara, P. Borthakur, B. L. Ouay and M. R. Das, *Chem. Eng. J.,* **2023**, 474, 145797. doi:10.1016/j.cej.2023.145797.

7 F. Manea, F. B. Houillon, L. Pasquato and P. Scrimin, *Angew. Chem. Int. Ed.,* **2004**, 43(45), 6165–6169. doi:10.1002/anie.200460649.

8 J. Wu, X. Wang, Q. Wang, Z. Lou, S. Li and Y. Zhu, *Chem. Soc. Rev.,* **2018**, 48(4), 1004–1076. doi:10.1039/c8cs00457a.

9 J. Li, H. Wei, S. Guo and E. Wang, *Anal. Chim. Acta,* **2008**, 630(2), 181–185. doi:10.1016/j.aca.2008.10.004.

10 S. Ghayyem, A. Swaidan, A. Barras, M. Dolci, F. Faridbod and S. Szunerits, *Talanta,* **2021**, 226, 122082. doi:10.1016/j.talanta.2021.122082.

11 Y. Qi, J. Ma, F.R. Xiu and X. Gao, *Microchim. Acta,* **2021**, 188(8), 273 doi:10.1007/s00604-021-04942-7.

12 Q. Xue, X. Li, Y. Peng, P. Liu, H. Peng and X. Niu, *Microchim. Acta,* **2020**, 187(5), 263. doi:10.1007/s00604-020-04232-8.

13 D.C. Onwudiwe, N. Gobile, O.A. Oyewo and S.S. Makgato, *Results Eng.,* **2023**, 20, 101521.

14 M.P. Ravele, O.C. Olatunde, O.A. Oyewo, D.C. Onwudiwe, S.S. Makgato and A. Hosseini-Bandegharaei, *Discov. Chem.,* **2025**, 2, 303.

15 X. Wang, Q.Z. Li, Y. Zhao and X. Gao, *ACS Appl. Mater. Interfaces,* **2025,** 17(49), 66110-66150. https://doi.org/10.1021/acsami.5c15196

16 P. Borah, D.J. Baruah, R. Duarah and M.R. Das, *Chem. Commun.,* **2025**, 61(58), 10685-10715. https://doi.org/10.1039/D5CC00180C

17 O.A. Oyewo and S.S. Makgato, *J,* **2023**, *6*, 564-578.

View Article Online
DOI: 10.1039/D5NA01116G

18 P. Li, Y. Li, M. Qi and X. Zhang, *Chem. Eng. J.,* **2024**, 493, 152686. https://doi.org/10.1016/j.cej.2024.152686

19 Z. Wen, J. Ke, J. Xu, S. Guo, Y. Zhang and R. Chen, *Chem. Eng. J.,* **2018**, 343, 416-426. https://doi.org/10.1016/j.cej.2018.03.034

20 C. Wang, M. Huang, W. Lou, W. Xiang, T. Zhou, J. Mao, F. Zan and X. Wu, *Chem. Eng. J.,* **2022**, 434, 134575. https://doi.org/10.1016/j.cej.2022.134575

21 Z. Zhao, H. An, J. Lin, M. Feng, V. Murugadoss, T. Ding, H. Liu, Q. Shao, X. Mai, N. Wang and H. Gu, *Chem. Rec.,* **2019**, 19, 873-882. https://doi.org/10.1002/tcr.201800153

22 M. Rashid, D. Mowla, F. Esmaeilzadeh, K. Dashtian and M. Bahmani, *J. Clean. Prod.,* **2021**, 317, 128471. https://doi.org/10.1016/j.jclepro.2021.128471

23 H. Lee, Y. Park, K. Song and J.Y. Park, *Acc. Chem. Res.,* **2022**, 55, 3727-3737. https://doi.org/10.1021/acs.accounts.2c00623

24 S. Li, J. Yang, X. Ruan, X. Cui and S.K. Ravi, *Adv. Funct. Mater.* **2026**, 36, 2503186. https://doi.org/10.1002/adfm.202503186

25 P. Babu, H. Park and J.Y. Park, *Surf. Sci. Technol.*, **2023**, 1(1), 29. https://doi.org/10.1007/s44251-023-00026-1

26 P. Babu and B. Naik, *Inorg. Chem.,* **2020**, 59, 10824-10834. https://doi.org/10.1021/acs.inorgchem.0c01325

27 U.P. Gawai, S.D. Kamble, S.K. Gurav, M.N. Singh, A.K. Yadav, S.N. Jha, N.P. Lalla, M.R. Bodke, M.D. Shirsat and B. Dole, *ACS Omega,* **2022**, 7, 6700-6709. https://doi.org/10.1021/acsomega.1c06179

28 P. Babu, S. Mohanty, B. Naik and K. Parida, *ACS Appl. Energy Mater.*, 2018, 1(11), 5936–5947

29 P. Babu, S. Mohanty, B. Naik and K. Parida, *Inorg. Chem.*, 2019, 58(18), 12480–12491.

30 J. Li, X. Zhao, J. Liu, L. Zhang and C. Yang, *J. Alloys Compd.,* **2019**, 777, 954-962. https://doi.org/10.1016/j.jallcom.2018.10.204

31 A. Manalu, K. Tarigan, S. Humaidi, M. Ginting, K. Sebayang, M. Rianna, M. Hamid, A. Subhan, P. Sebayang and I.P. Manalu, *Int. J. Electrochem. Sci.,* **2022**, 17(3), 22036. https://doi.org/10.20964/2022.03.11

32 Y. Hou, C. Hou, Y. Zhai, H. Li, T. Chen, Y. Fan, H. Wang and W. Wang, *Electrochim. Acta,* **2019**, 324, 134884. https://doi.org/10.1016/j.seppur.2025.132072

View Article Online
DOI: 10.1039/D5NA01116G

33 D. Pradhan, P.K. Panda, A. Mishra, E. Falletta, S.K. Dash, *Environ. Quality Management,* **2022**, 32(2), 85-100. https://doi.org/10.1002/tqem.21916

34 J. Oliva, C. Gomez-Solis, L.A. Diaz-Torres, A. Martinez-Luevanos, A.I. Martinez and E. Coutiño-Gonzalez, *J. Phys. Chem. C* **2018**, 122(3), 1477-1485. https://doi.org/10.1021/acs.jpcc.7b10375

35 F.T.L. Muniz, M.R. Miranda, C. Morilla dos Santos and J.M. Sasaki, *Acta Crystallogr., Sect. A: Found. Crystallogr.,* **2016**, 72, 385-390. https://doi.org/10.1107/S205327331600365X

36 P. Babu, S. Mohanty, B. Naik and K. Parida, *ACS Appl. Energy Mater.,* **2018**, 1, 5936-5947.

37 P. Babu, S. Mohanty, B. Naik and K. Parida, *Inorg. Chem.,* **2019**, 58, 12480-12491.

38 N. Hoque, S. Lee, Y.B. Park, S. Roy, M.J. Baruah, S. Biswas, G. Gogoi, T.J. Bora, R. Dutta and K.K. Bania, *ChemNanoMat,* **2022**, 8(10), e202200280. https://doi.org/10.1002/cnma.202200280

39 N. Hoque, M.J. Baruah, A.H. Biman, S. Biswas, G. Gogoi, R. Dutta and K.K. Bania, *ACS Appl. Energy Mater.,* **2022**, 5, 6118-6128. https://doi.org/10.1021/acsaem.2c00523

40 M.J. Baruah, T.J. Bora, G. Gogoi, N. Hoque, N.K. Gour, S.K. Bhargava, A.K. Guha, J.K. Nath, B. Das and K.K. Bania, *J. Colloid Interface Sci.,* **2022**, 608, 1526-1542. https://doi.org/10.1016/j.jcis.2021.10.091

41 C. Zhao, M. Li, H. Guo, X. Tong, W. Gao and C. Zhao, *J. Energy Storage*, **2024**, 84, 110950.

42 T.J. Frankcombe and Y. Liu, *Chem. Mater.,* **2023**, 35(14), 5468-5474.

43 L. A. Marquez and H. B. Dunford, *Biochem.,* **1997**, 36(31), 9349–9355. doi:10.1021/bi970595j.

44 A. K. Dutta, S. K. Maji, D. N. Srivastava, A. Mondal, P. Biswas and P. Paul, *ACS Appl. Mater. Interfaces,* **2012**, 4(4), 1919–1927. doi:10.1021/am300408r.

45 P. Borthakur, G. Darabdhara, M.R. Das, R. Boukherroub and Szunerits, S., *Sens. Actuators B Chem.,* **2017**, 244, 684-692.

46 P.K. Boruah, G. Darabdhara, P. Borthakur, B. Le Ouay and M.R. Das, *Chem. Eng. J.* **2023**, 474, 145797.

47 M. Li, H. Zhang, Y. Hou, X. Wang, C. Xue, W. Li, *Nanoscale Horiz.,* **2019**, 5, 202–217. doi:10.1039/c9nh00577c.

View Article Online
DOI: 10.1039/D5NA01116G

48 F. Jiang, Z. Zheng, Z. Xu, S. Zheng, Z. Guo and L. Chen, *J. Hazard. Mater.,* **2005**, 134, 94–103. doi:10.1016/j.jhazmat.2005.10.041.

49 W. Zou, Y. Tang, H. Zeng, C. Wang and Y. Wu, *J. Hazard. Mater.* **2021**, 417, 125994. doi:10.1016/j.jhazmat.2021.125994.

50 J. Shen, S. Shang, X. Chen, D. Wang and Y. Cai, *Sens. Actuators B Chem.*, **2017**, 248, 92–100. doi:10.1016/j.snb.2017.03.123.

51 D. Zhang, Z. Dong, X. Jiang, M. Feng, W. Li and G. Gao, *Anal. Methods,* **2013**, 5, 1669. doi:10.1039/c3ay26555b.

52 P. M. Carrasco, I. García, L. Yate, R. T. Zaera, G. Cabañero and H. J. Grande, *Carbon,* **2016**, 109, 658–665. doi:10.1016/j.carbon.2016.08.038.

53 K. Feke, M. T. Alula, H. Spende, A. Waag and P. Lemmens, *J. Cluster Sci.,* **2022**, 34, 1009–1018. doi:10.1007/s10876-022-02284-9.

54 Y. Cheng, P. Shen, X. Li, X. Li, K. Chu and Y. Guo, *Sens. Actuators B Chem.* **2022**, 376, 132979. doi:10.1016/j.snb.2022.132979.

55 S. Kulandaivel, W.C. Lo, C.H. Lin and Y.C. Yeh, *Anal. Chim. Acta*, **2022**, 1227, 340335. doi:10.1016/j.aca.2022.340335.

56 X. Guo, F. Yang, L. Jing, J. Li, Y. Li and R. Ding, *J. Hazard. Mater.,* **2022**, 431, 128621. doi:10.1016/j.jhazmat.2022.128621.

The data supporting the findings of this study are available from the corresponding author upon request.

View Article Online
DOI: 10.1039/D5NA01116G